JGP Journal of General Physiology

ARTICLE

Excitation–Contraction Coupling

Pannexin-1 and $Ca_V1.1$ show reciprocal interaction during excitation–contraction and excitation–transcription coupling in skeletal muscle

Francisco Jaque-Fernández[1], Gonzalo Jorquera[1,3], Jennifer Troc-Gajardo[1], France Pietri-Rouxel[4], Christel Gentil[4], Sonja Buvinic[6], Bruno Allard[5], Enrique Jaimovich[1,2], Vincent Jacquemond[5], and Mariana Casas[1,2]

One of the most important functions of skeletal muscle is to respond to nerve stimuli by contracting. This function ensures body movement but also participates in other important physiological roles, like regulation of glucose homeostasis. Muscle activity is closely regulated to adapt to different demands and shows a plasticity that relies on both transcriptional activity and nerve stimuli. These two processes, both dependent on depolarization of the plasma membrane, have so far been regarded as separated and independent processes due to a lack of evidence of common protein partners or molecular mechanisms. In this study, we reveal intimate functional interactions between the process of excitation-induced contraction and the process of excitation-induced transcriptional activity in skeletal muscle. We show that the plasma membrane voltage-sensing protein $Ca_V1.1$ and the ATP-releasing channel Pannexin-1 (Panx1) regulate each other in a reciprocal manner, playing roles in both processes. Specifically, knockdown of $Ca_V1.1$ produces chronically elevated extracellular ATP concentrations at rest, consistent with disruption of the normal control of Panx1 activity. Conversely, knockdown of Panx1 affects not only activation of transcription but also $Ca_V1.1$ function on the control of muscle fiber contraction. Altogether, our results establish the presence of bidirectional functional regulations between the molecular machineries involved in the control of contraction and transcription induced by membrane depolarization of adult muscle fibers. Our results are important for an integrative understanding of skeletal muscle function and may impact our understanding of several neuromuscular diseases.

Introduction

Besides its role in energy transfer, ATP is known to operate as an extracellular messenger for autocrine and paracrine signaling (Corriden and Insel, 2010). Specifically, in a variety of cell types, including muscle cells, ATP can be released across the plasma membrane into the extracellular medium through pannexin channels (D'hondt et al., 2011). Pannexin-1 is an integral membrane glycoprotein that belongs to a family of proteins encoded by three genes in vertebrates (*Panx1*, *Panx2*, and *Panx3*). A widespread tissue distribution of Panx1 has been established, with highest levels found in skeletal muscle (Baranova et al., 2004).

Roles for Panx1 have been described in a variety of physiological and pathological processes, including propagation of intercellular Ca^{2+} (Locovei et al., 2006), afferent neurotransmission (Romanov et al., 2007), activation of the inflammasome (Silverman et al., 2009), recruitment of macrophages to apoptotic cells (Chekeni et al., 2010), pressure overload–induced fibrosis in the heart (Nishida et al., 2008), and ionic dysregulation during stroke-induced ischemic neuronal death (Thompson et al., 2006). Panx1 has also been shown to contribute to epileptic-form seizure activity (Thompson

[1]Programa de Fisiología y Biofísica, Facultad de Medicina, Instituto de Ciencias Biomédicas, Universidad de Chile, Santiago, Chile; [2]Center for Exercise, Metabolism and Cancer, Facultad de Medicina, Instituto de Ciencias Biomédicas, Universidad de Chile, Santiago, Chile; [3]Centro de Neurobiología y Fisiopatología Integrativa, Instituto de Fisiología, Facultad de Ciencias, Universidad de Valparaíso, Valparaíso, Chile; [4]Université Pierre et Marie Curie, Université Paris 06, Institut National de la Santé et de la Recherche Médicale/Centre National de la Recherche Scientifique/Institut de Myologie/Centre de Recherche en Myologie, Groupement hospitalier universitaire Pitié Salpêtrière, Paris, France; [5]Université Lyon, Université Claude Bernard Lyon 1, Centre National de la Recherche Scientifique UMR-5310, Institut National de la Santé et de la Recherche Médicale U-1217, Institut NeuroMyoGène, Lyon, France; [6]Institute for Research in Dental Sciences, Faculty of Dentistry, Universidad de Chile, Santiago, Chile.

Correspondence to Mariana Casas: mcasas@med.uchile.cl

This work is part of a special issue on excitation–contraction coupling.

et al., 2008). The opening of the Panx1 channel is essential to its function, and any deregulation leading to uncontrolled opening may cause cell death (Thompson et al., 2006). Thus, a robust mechanism controlling the opening and closure of Panx1 is of vital importance to the cells. Along this line, Panx1 channels are known to be potentially activated by different stimuli, including mechanical stress (Bao et al., 2004), elevation of intracellular [Ca^{2+}] (Locovei et al., 2006), activation of P2Y purinergic receptors (Locovei et al., 2006; Pelegrin and Surprenant, 2006), and ischemic or hypoxic conditions (Sridharan et al., 2010; Thompson et al., 2006). Despite the high level of expression of Panx1 in differentiated muscle, its role in this tissue has remained obscure until Panx1 was found to be involved in an interaction with the membrane protein $Ca_V1.1$ (Arias-Calderón et al., 2016; Jorquera et al., 2013).

$Ca_V1.1$ is the voltage sensor for skeletal muscle excitation–contraction (EC) coupling. Upon membrane depolarization, it undergoes conformational changes that trigger the opening of ryanodine receptor 1 (RYR1) channels in the SR membrane through protein–protein conformational coupling; this generates a rise in cytosolic [Ca^{2+}] that activates contraction (see Ríos and Pizarro, 1991; Schneider, 1994). The coupling of $Ca_V1.1$ with RYR1 is a peculiar case, because beyond the orthograde control that $Ca_V1.1$ exerts over RYR1 activity, there is also a retrograde control of $Ca_V1.1$ by RYR1 (Andronache et al., 2009; Bannister and Beam, 2009; Estève et al., 2010; Nakai et al., 1996). These two proteins interact physically and functionally to make the robust complex that ensures EC coupling (Beam and Bannister, 2010; Paolini et al., 2004; Rebbeck et al., 2014; Rios and Brum, 1987; Samsó, 2015).

$Ca_V1.1$ also operates as a voltage-gated Ca^{2+} channel responsible for a slow Ca^{2+} entry across the transverse tubule (t-tubule) membrane upon membrane depolarization (Ríos and Pizarro, 1991; Tanabe et al., 1990). Although not essential for EC coupling (Dayal et al., 2017), there is evidence that this Ca^{2+} entry contributes to refilling of the SR Ca^{2+} store (Lee et al., 2015; Robin and Allard, 2015) and that it is also coupled to CaMKII activation, with a consequent impact on downstream signaling pathways affecting muscle metabolism (Georgiou et al., 2015; Lee et al., 2015).

A third role for $Ca_V1.1$ was demonstrated in recent years as a trigger for activation of a frequency-dependent signaling cascade related to excitation–transcription (ET) coupling, where $Ca_V1.1$ voltage-sensing activity is coupled to activation of ATP release out of the muscle cells through Panx1 channels after electrical stimulation (ES) in a frequency-dependent manner (Arias-Calderón et al., 2016; Buvinic et al., 2009; Jorquera et al., 2013). Released ATP binds purinergic receptors, which activate a signaling cascade responsible for changes in the transcriptional activity of genes involved in muscle plasticity. Moreover, ES-dependent ATP release is practically absent in cultured muscle cells lacking $Ca_V1.1$, and the $Ca_V1.1$ blocker nifedipine completely abolishes both ATP release and transcriptional activity produced by a permissive frequency of ES in adult muscle fibers (Casas et al., 2014; Jorquera et al., 2013). It has been shown that Panx1 is in close proximity to several proteins related to ET coupling, including $Ca_V1.1$ (Arias-Calderón et al., 2016; Jorquera et al., 2013) and P2Y2 (Arias-Calderón et al., 2016).

In recent years, knockdown or expression of mutated forms of other proteins has been shown to affect $Ca_V1.1$ membrane expression and/or functional features of $Ca_V1.1$ via EC coupling. Notably, it has been established that in addition to $Ca_V1.1$ and RYR1, β1a, Stac3, and junctophilin-2 are necessary for activation of EC coupling in skeletal muscle (Couchoux et al., 2007; Golini et al., 2011; Mosca et al., 2013; Perni et al., 2017; Polster et al., 2016; Weiss et al., 2008). Other proteins can also modulate $Ca_V1.1$ activity, including Cav3, JP-45, and junctophilin-1, altering calcium current and/or activation of intracellular Ca^{2+}-release (Anderson et al., 2006; Weiss et al., 2008).

In the present work, we propose that Panx1 belongs to the family of proteins that are functional interacting partners of $Ca_V1.1$, affecting its role in ET and EC coupling. Indeed, a reduction of Panx1 alters $Ca_V1.1$ Ca^{2+} channel properties, compromises the EC coupling function, and impairs transcriptional activation of target genes after low-frequency ES of fully differentiated muscle fibers. Moreover, we show that Panx1 and $Ca_V1.1$ may also be reciprocal partners capable of mutually regulating their respective function, because a reduction in $Ca_V1.1$ content alters Panx1 proper control of ATP release, consequently affecting transcriptional activity.

Materials and methods

Ethical approval

All experiments and procedures were conducted in accordance with the guidelines of the local animal ethics committee of the University of Chile, University Paris 06, University Claude Bernard Lyon 1, the French Ministry of Agriculture (decree 87/848), and the revised European Directive 2010/63/EU.

Down-expression of Pannexin-1 in muscle fibers

Adeno-associated virus (AAV)-mCherry-U6-mPANX1-shRNA plasmid was obtained from Vector Biolabs. It targets a specific sequence of mouse Panx1 and has been validated for ∼90% knockdown of mRNA in B16-F0 cells.

Exogenous expression by electroporation was performed in the *flexor digitorum brevis* (*fdb*) muscles of 6–7-wk-old Swiss OF1 (charge movement measurements) or BalbC (Ca^{2+} current and Ca^{2+} release measurements) male mice using a general procedure previously described (Legrand et al., 2008). Mice were anaesthetized either by isoflurane inhalation (3% in air, 300 ml/min) using a commercial delivery system (Univentor 400 Anesthesia Unit; Uninventor) or intraperitoneal injection of a mix of 0.1 g/kg ketamine and 0.01 g/kg xylazine. 25 µl of a solution containing 2 mg/ml hyaluronidase dissolved in sterile saline were then injected into the footpads of each hind paw. 40 min later, the mouse was reanaesthetized using the same procedure as for hyaluronidase injection. A 20-µl volume of Tyrode solution containing 1 µg/µl mCherry DNA was injected into the footpad of a hindpaw, whereas the same volume of solution containing 1 µg/µl shRNA-Panx1 DNA was injected into the footpad of the contralateral hindpaw. Following the injections, two gold-plated stainless-steel acupuncture needles connected to the electroporation apparatus were inserted under the skin, near the proximal and distal portion of the foot, respectively.

The standard protocol used consisted in 20 pulses of 100 V/cm amplitude and 20 ms duration delivered at a frequency of 1 Hz by a BTX ECM 830 square-wave pulse generator (Harvard Apparatus; Holliston). Experimental observations and measurements were performed 2 wk later. Fibers positive for mCherry that were isolated from muscles transfected with shRNA-Panx1 and muscles transfected with mCherry only are referred to as shRNA-Panx1 and corresponding control fibers, respectively.

Down-expression of $Ca_V1.1$ in muscle fibers

Down-expression of α1s subunit of dihydropyridine receptor (DHPR) was achieved by a U7 exon-skipping strategy using AAV vectors (AAV-U7delα1s). Previously designed antisense sequence and control nonfunctional construct were used as described earlier (Piétri-Rouxel et al., 2010). In brief, adult C57/Black6 mice were anaesthetized with a mix of 0.1 g/kg ketamine and 0.01 g/kg xylazine. Two intramuscular injections in 24 h of a mixture containing AAV (U7-SA) and AAV (U7-ESE) were performed in one footpad, and the contralateral footpad was injected with the control AAV (U7-Ctrl). Experimental measurements were performed 4 mo later. Fibers isolated from muscles treated with the active AAV and the nonfunctional construct are referred to as ΔDHPR and corresponding control fibers as WT, respectively.

Preparation of isolated muscle fibers for electrophysiology and Ca^{2+} measurements

Single fibers were isolated from the *fdb* muscles using a previously described procedure (Jacquemond, 1997). In brief, mice were euthanized by cervical dislocation before removal of the muscles. Muscles were treated with collagenase (type 1; Sigma-Aldrich) for 60 min at 37°C. Single fibers were then obtained by dissociating the muscles within the experimental chamber. Fibers were dispersed on the glass bottom of a 50-mm-wide culture μ-dish (Ibidi). Fibers were first partially insulated with silicone grease, as described previously (Jacquemond, 1997), so that only a portion of the fiber extremity was left out of the silicone. All experiments were performed at room temperature (20–22°C).

Extracellular ATP measurement

50 μl of extracellular media aliquots from fiber plates was removed at different times. ATP concentrations were measured with the CellTiter-Glo Luminescent Cell Viability Assay (Promega), as reported (Jorquera et al., 2013). Data were calculated as picomoles extracellular ATP per microgram total RNA, and the ratios between experimental versus control points were reported. Normalization by total RNA instead of total protein was chosen, because adult muscle fibers were seeded on a Matrigel-coated surface (containing a large amount of protein), which may affect the protein determination associated with fibers only. Total RNA was obtained from skeletal muscle fibers using Trizol reagent (Invitrogen) according to the manufacturer's protocol.

Real-time PCR

Total RNA was obtained from skeletal muscle fibers using Trizol reagent (Invitrogen) according to the manufacturer's protocol. cDNA was prepared from 1 μg RNA using SuperScript II enzyme (Invitrogen), according to the manufacturer's protocol. Real-time PCR was performed using Stratagene Mx3000P (Stratagene) using the Brilliant III Ultra-Fast QPCR and QRT-PCR Master Mix amplification kit (Agilent Technologies). The following primers were used: slow isoform of troponin I (TnIs), 5′-GAGGTTGTGGGCTTGCTGTATGA-3′ (sense), 5′-GGAGCGCATATTAGGGATGT-3′ (antisense); fast isoform of TnI (TnIf), 5′-AGGTGAAGGTGCAGAAGAGC-3′ (sense), 5′-TTGCCCCTCAGGTCAAATAG-3′ (antisense); β-actin, 5′-TACAATGAGCTGCGTGTG-3′ (sense), 5′-TACATGGCTGGGGTGTTGAA-3′ (antisense); and P0, 5′-CTCCAAGCAGATGCAGCAGA-3′ (sense), 5′-ATAGCCTTGCGCATCATGGT-3′ (antisense). All primers used presented optimal amplification efficiency (between 90% and 110%). PCR amplification of the housekeeping gene β-actin or P0 was performed as control. Thermocycling conditions were as follows: 95°C for 3 min and 40 cycles of 95°C for 10 s, 60°C for 20 s. Expression values were normalized to β-actin or P0 and reported in units of $2^{-\Delta\Delta CT}$ ± SEM. Cycle threshold (CT) value was determined by MXPro software when fluorescence was 25% higher than background. PCR products were verified by melting-curve analysis.

Western blot analysis

Muscles were lysed in 60 μl ice-cold lysis buffer (20 mM Tris-HCl, pH 7.4, 1% Triton X-100, 2 mM EDTA, 10 mM Na_3VO_4, 20 mM NaF, 10 mM sodium pyrophosphate, 150 mM NaCl, 1 mM PMSF, and a protease inhibitor mixture). 30 μg of total protein from cell lysates were separated in 10% SDS-polyacrylamide gels and transferred to polyvinylidene difluoride membranes (Millipore). Membranes were blocked at room temperature for 1 h in Tris-buffered saline containing 3% fat-free milk, with or without 0.5% Tween 20, and then incubated overnight with the appropriate primary antibody. For $Ca_V1.1$, a mouse monoclonal antibody (1:2,000) from Abcam (ab2862) was used (Hu et al., 2015). For Panx-1, a rabbit polyclonal antibody (1:10,000) from Thermo Fisher Scientific (catalog no. 487900) was used (Melhorn et al., 2013). α-Actin (1:1,000) from Sigma-Aldrich (a2066; Mormeneo et al., 2012) or β-tubulin from Cell Signaling (11H10; Gallot et al., 2017) were used as charge control for normalization of different lanes.

Membranes were incubated with the appropriate secondary antibody at room temperature for 1.5 h. The immunoreactive proteins were detected using ECL reagents according to the manufacturer's instructions. For loading control, membranes were stripped in buffer containing 0.2 M glycine (pH 2) and 0.05% Tween 20, at room temperature for 30 min, blocked as described previously, and assessed with the corresponding control antibody.

Electrophysiology

Whole-cell voltage-clamp experiments were performed. For measurements of DHPR Ca^{2+} current and intracellular Ca^{2+} transients in fibers expressing shRNA-Panx1 and/or mCherry, an Axopatch 200B patch-clamp amplifier (Molecular Devices) was used, and data acquisition and command voltage pulse generation were achieved with a Digidata 1322A analogue-digital, digital-analogue converter

(Axon Instruments) controlled by pClamp software (Axon Instruments). For measurements of DHPR Ca^{2+} current in fibers down-expressing $Ca_V1.1$, an RK-400 patch-clamp amplifier (Bio-Logic) was used in combination with a Digidata 1322A converter (Axon Instruments) controlled by pClamp software (Axon Instruments). For measurements of intracellular Ca^{2+} transients in fibers down-expressing $Ca_V1.1$ and measurements of intramembrane charge movement in fibers expressing shRNA-Panx1 and/or mCherry, an RK-400 patch-clamp amplifier (Bio-Logic) was used in combination with a BNC-2120 converter (National Instruments) controlled by WinWCP software (University of Strathclyde). Fibers were bathed in a TEA-containing extracellular solution (see Solutions). Voltage clamp was performed with a micropipette filled with the intracellular-like solution (see Solutions). The tip of the micropipette was inserted through the silicone within the insulated part of the fiber, and it was slightly crushed against the bottom of the chamber in order to decrease the access resistance. Analogue compensation was adjusted to further decrease the effective series resistance. Membrane-depolarizing steps were applied from a holding command potential of −80 mV. The $Ca_V1.1$ Ca^{2+} current was measured in response to 0.5-s-long depolarizing steps of increasing level. The linear leak component of the current was removed by subtracting the adequately scaled value of the steady current measured during a 20-mV hyperpolarizing step. Peak current values were normalized by the fiber capacitance (ampere/farad, A/F). The voltage dependence of the peak current was fitted with the following equation:

$$I(V) = Gmax(V - Vrev)/[1 + exp(V0.5\text{-}V)/k], \quad (1)$$

where I(V) is the peak current density at the command voltage V, Gmax is the maximum conductance normalized to the capacitance of the fiber (siemens/farad, S/F), Vrev is the apparent reversal potential, V0.5 is the half-activation potential, and k is the steepness factor. It should be stressed that Ca^{2+} current measurements designed to test the consequences of Pannexin-1 down-expression and $Ca_V1.1$ down-expression, respectively, were performed on muscle fibers from mice of different strains and age and under slightly differing conditions, which explains the difference in current density between the two data groups.

Intramembrane charge movement currents were measured and analyzed according to previously described procedures (Collet et al., 2003; Pouvreau et al., 2004). In brief, adequately scaled control current records elicited by 50-ms-long hyperpolarizing pulses of 20 mV were subtracted from the current elicited by test depolarizing pulses of the same duration to various levels. In a few cases, test records were further corrected for a sloping baseline using previously described procedures (Horowicz and Schneider, 1981). The amount of charge moved during a test pulse was measured by integrating the on and off portion of the corrected test current records. The calculated charge was normalized to the capacitance of the fiber. The steady-state distribution of the normalized charge was fitted with a two-state Boltzmann function:

$$Q(V) = Qmax/\{1 + \exp[(V0.5 - V)/k]\}, \quad (2)$$

where Qmax corresponds to the maximally available charge, V0.5 is the voltage of equal charge distribution, and k is the steepness factor.

Intracellular Ca^{2+} measurements

Voltage-activated Ca^{2+} transients in fibers expressing shRNA-Panx1 and/or mCherry were measured with the dye fluo-4. For this, muscle fibers were equilibrated for 30 min in the presence of 10 µM fluo-4 AM before establishing the silicone voltage-clamp conditions. Fluo-4 Ca^{2+} transients were measured with the line-scan mode (1.53 ms per line) of a Zeiss LSM 710 confocal microscope. The dye was excited with the 488-nm line of the argon laser, and a 505–530-nm band pass filter was used on the detection channel. Fluo-4 Ca^{2+} transients were expressed as F/F0, where F0 is the background-corrected baseline fluorescence.

Voltage-activated Ca^{2+} transients in fibers down-expressing $Ca_V1.1$ and corresponding control fibers were measured with the dye indo-1 following previously described procedures (Pouvreau et al., 2004; Weiss et al., 2010). In brief, before voltage clamp, the Ca^{2+} sensitive dye indo-1 was introduced locally into the fiber by pressure microinjection through a micropipette containing 1 mM indo-1 dissolved in the intracellular-like solution (see Solutions). Fibers were then left for 1 h to allow for intracellular equilibration. Indo-1 fluorescence was measured on an inverted Nikon Diaphot epifluorescence microscope equipped with a commercial optical system allowing simultaneous detection of fluorescence at 405 nm (F405) and 485 nm (F485) by two photomultipliers (IonOptix) upon excitation at 360 nm. The standard ratio method was used to calculate $[Ca^{2+}]$ from R = F405/F485, with in vivo values for the calibration parameters Rmin (the value or R in the absence of Ca^{2+}), Rmax (the value of R in the presence of a Ca^{2+} concentration saturating indo-1), KD (the apparent dissociation constant for Ca^{2+} binding to indo-1), and β (the value for the ratio of F485 in the absence of Ca^{2+} to F485 in the presence of a saturating Ca^{2+} concentration), determined as previously described (Jacquemond, 1997).

This same setup and related procedures were also used to estimate the SR Ca^{2+} content in fibers expressing shRNA-Panx1 and/or mCherry using a method described by (Al-Qusairi et al., 2009). For this, muscle fibers were equilibrated for 30 min with the voltage-clamp pipette intracellular-like solution also containing indo-1 and EGTA (see Solutions). Then, 50-ms-long depolarizing pulses from −80 to +10 mV were applied, before and after applying 50 µM cyclopiazonic acid (CPA) in the extracellular medium, using a thin polyethylene capillary perfusion system operating by gravity. The maximum change in baseline indo-1 saturation level following pulses delivered in the presence of CPA was taken as an index of the SR Ca^{2+} content.

Solutions

The standard intracellular-like solution used in the voltage-clamp pipette contained (in mM) 140 K-glutamate, 5 Na2-ATP, 5 Na2-phosphocreatine, 5.5 $MgCl_2$, 5 glucose, and 5 HEPES. For $Ca_V1.1$ Ca^{2+} current measurements in fibers expressing shRNA-Panx1 and/or mCherry, this solution also contained 20 mM EGTA. For the experiments aimed at estimating the SR Ca^{2+} content in fibers expressing shRNA-Panx1 and/or mCherry, the standard intracellular-like solution also contained 0.2 mM indo-1, 20 mM EGTA, and 8 mM $CaCl_2$. For intramembrane charge movement, the intra-pipette solution contained (in mM)

140 TEA-methanesulfonate, 5 Na2-ATP, 5 Na2-phosphocreatine, 5.5 $MgCl_2$, 5 glucose, 20 EGTA, and 5 HEPES.

The standard extracellular solution contained (in mM) 140 TEA-methanesulfonate, 2.5 $CaCl_2$, 2 $MgCl_2$, 1 4-aminopyridine, 10 TEA-HEPES, and 0.002 tetrodotoxin. For $Ca_V1.1$ Ca^{2+} current measurements in fibers down-expressing $Ca_V1.1$ and corresponding control fibers, the standard solution also contained EGTA-AM (5 µM). For Ca^{2+} measurements with fluo-4, 50 µM N-benzyl-p-toluene sulphonamide was added to the standard solution. For intramembrane charge movement the extracellular solution contained 140 TEA-methanesulfonate, 0.1 $CaCl_2$, 1 $MnCl_2$, 1 $CdCl_2$, 1 4-aminopyridine, 10 TEA-HEPES, and 0.002 tetrodotoxin. All solutions were adjusted to pH 7.20.

Statistics

Statistical analysis was performed using Microcal Origin, version 8.0 (OriginLab) and GraphPad Prism 9. Least-squares fits were performed using a Marquardt–Levenberg algorithm routine included in Microcal Origin. Data values are presented as means ± SEM for *n* animals. Statistical differences were determined assuming significance for $P < 0.05$ (*/≠, $P < 0.05$; **/≠≠, $P < 0.01$; ***, $P < 0.005$; ****, $P < 0.001$). If groups followed a normal distribution, a Student's *t* test was applied. When, even normally distributed, they do not have the same SD, the *t* test was followed by a Welch's correction. When data were not normally distributed, Kruskal–Wallis or Mann–Whitney tests were applied. For the case of electrophysiological measurement, we performed a nested analysis of the data following instruction given in Eisner (2021), where *N* is the number of animals and *n* is the number of fibers from each animal. Numbers of individual measurements and individual animals used are mentioned in the figure legends.

Results

Down-expression of $Ca_V1.1$ in adult muscle fibers alters the function of Pannexin-1

We have described that ATP release through Panx1 is activated by $Ca_V1.1$ at low frequencies of ES in adult muscle fibers (Casas et al., 2010; Jorquera et al., 2013). To study a possible change in Panx1 activity induced by the loss of $Ca_V1.1$ in adult muscle, we used a model of down-expression of $Ca_V1.1$, taking advantage of a U7 exon-skipping strategy (Piétri-Rouxel et al., 2010). In these muscles (ΔDHPR), we observed a reduction of 60% in protein levels of $Ca_V1.1$ (Fig. 1 A). Importantly, in these fibers down-expressing $Ca_V1.1$, we observed increased basal levels of ATP release (Fig. 1 B), indicating a deregulation of the normally closed configuration of Panx1 channel in resting conditions. After ES, ΔDHPR fibers did not show an increase in extracellular ATP levels compared with control fibers (Fig. 1 B). An extreme example of the absence of $Ca_V1.1$ is the muscular dysgenesis (mdg) muscle cell, originally obtained from dysgenic mice not expressing $Ca_V1.1$. These cells showed to have increased values of basal ATP release compared with WT myotubes, and this release was inhibited by incubation with 5 µM carbenoxolone (Fig. 1 C), indicating that ATP release occurs via Panx1 channels. Accordingly, in ΔDHPR fibers, the maintained increase in basal extracellular ATP levels, induced an increase in mRNA levels of TnIs and a decrease in mRNA levels of the fast isoform of this gene (TnIf; Fig. 1 D), a phenomenon previously seen in fibers stimulated with 20 Hz ES or in fibers exposed to 30 µM external ATP (Jorquera et al., 2013). It is important to mention that 4 h after ES, ΔDHPR fibers did not show changes in mRNA levels of TnI isoforms compared with unstimulated fibers (Fig. 1 D).

To check the functional consequences of $Ca_V1.1$ down-expression, voltage-activated Ca^{2+} current and cytosolic Ca^{2+} transients were measured in a separate set of muscle fibers from control and U7 exon-treated muscles 4 mo following AAV transduction. Fig. 2 A shows representative Ca^{2+} current traces from a control fiber and from a U7 exon–skipped fiber. Fig. 2 B shows the mean values for peak Ca^{2+} current density versus voltage in the two populations of fibers. Fitting the individual series of data points in each fiber with Eq. 1 gave mean values for Gmax, Vrev, V0.5, and k of 234 ± 19 S/F, 68 ± 2 mV, 5 ± 1 mV, and 6 ± 0.4 mV and 166 ± 14 S/F, 69 ± 3 mV, 3 ± 1 mV, and 5 ± 0.4 mV in control ($n = 14$, from $n = 4$ mice) and U7 exon–skipped fibers ($n = 14$, from $n = 4$ mice), respectively (Fig. 2 B, right panel). There was a significant ∼30% reduction in the maximal conductance in the U7 exon–skipped fibers. For this significant variation (Gmax), we made a nested analysis that conclude the same significant difference in Gmax between two groups. The left panel in Fig. 2 C shows indo-1 Ca^{2+} transients from a control fiber and from a U7 exon–skipped fiber obtained in response to depolarizing pulses from −80 to +10 mV of 20 ms duration. Resting $[Ca^{2+}]$ level did not differ between the two groups of fibers (Fig. 2 C, right). Also, fitting a single exponential function to the decay of the Ca^{2+} transients showed no significant difference in the mean values between control and U7 exon–skipped fibers, suggesting that the Ca^{2+} removal capabilities of the fibers were unaffected (mean τ values were 48.2 ± 9 and 49.5 ± 13 ms in control and U7 exon–treated fibers, respectively). Conversely, the peak $[Ca^{2+}]$ level reached in response to a depolarizing pulse was significantly depressed in the U7 exon–skipped fibers (by 34%; Fig. 2 C, right). As above, for this significantly different set of data, we also made a nested analysis and found the same significant difference in peak $[Ca^{2+}]$ level between the two groups. Altogether, these results establish a significant alteration of the Ca^{2+} channel and EC coupling activity of $Ca_V1.1$ in fibers treated with the active AAV. The fact that the relative depression in Ca^{2+} current density was lower than the decrease in protein level (Fig. 1 A) was likely due to the use of different preparations of AAV in the two sets of experiments.

Down-expression of Pannexin-1 suppresses low-frequency ES-induced ATP release in adult muscle fibers

We first performed experiments to validate the Panx1 knockdown model. For this aim, we electroporated the AAV-mCherry-U6-mPANX1-shRNA plasmid (shPanx1) in the *fdb* muscles of mice. To distinguish the effects of Panx1 down-expression from possible consequences of electroporation and overexpression of a fluorescent protein, we electroporated a mCherry carrying plasmid in the muscle from the contralateral paw to use the corresponding fibers as controls. We waited for 2 wk to evaluate levels of expression of Panx1 and the consequent disturbance of ATP release induced after ES of fibers at 20 Hz (Jorquera et al.,

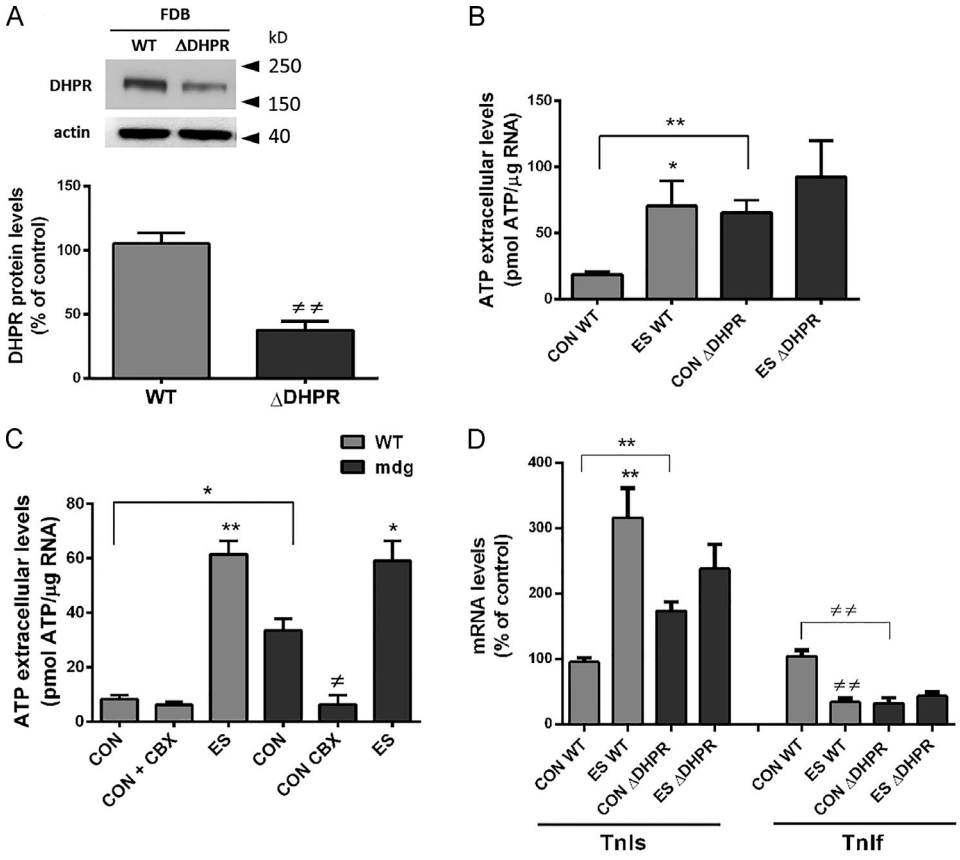

Figure 1. **Leaky behavior of Pannexin-1 in adult muscle fibers down-expressing $Ca_V1.1$, mimics the effect induced by ATP after ES of fibers at 20 Hz.** **(A)** $Ca_V1.1$ down-expression by the U7 exon–skipping strategy (ΔDHPR fibers) induces a reduction of >60% in $Ca_V1.1$ protein level. Top panel shows a representative blot image, while quantification of the reduction in $Ca_V1.1$ content is shown at the bottom (n = 3 *fdb* muscles from three distinct mice). FDB, *flexor digitorum brevis*. **(B)** Extracellular ATP levels was measured in basal condition (CON) and after ES in WT and ΔDHPR fibers. We observed an increase by more than three times of the basal extracellular ATP level in ΔDHPR muscle fibers compared with WT ones. WT and ΔDHPR fibers received ES consisted of 270 square pulses of 0.3-ms duration at 20 Hz. After ES, WT fibers experienced a significant increase in extracellular ATP levels; meanwhile, after ES, ΔDHPR fibers did not change extracellular ATP compared with CON condition (n = 3 cultures from three distinct mice). **(C)** A similar increase in basal extracellular ATP levels (CON) was observed in WT and lacking $Ca_V1.1$ (mdg) myotubes, which was suppressed by incubation with 5 μM of the Panx1 inhibitor carbenoxolone (CBX; n = 5 independent experiments). **(D)** Graph show that increased basal levels of mRNA for the slow isoform of TnI and decreased level for the fast isoform of TnI are observed in ΔDHPR *fdb* muscle fibers compared with WT fibers. 4 h after ES, TnIs mRNA levels increased, while TnIf mRNA levels diminished in WT fibers. ΔDHPR fibers did not show changes in TnIs and TnIf mRNA levels after ES (n = 4 cultures from four distinct mice). Gray bars represent WT muscles, and black bars represent ΔDHPR muscles. Significant differences within multiple groups were examined using a Kruskal–Wallis test for repeated measures, followed by a multiple comparison test. A Mann–Whitney test was used to detect significant differences between two groups. Data are expressed as mean ± SEM. */≠, $P < 0.05$; **/≠≠, $P < 0.01$.

2013). In Fig. 3 A, we show the expression of the mCherry reporter in muscles electroporated with the shPanx1 (carrying mCherry marker) and mCherry (alone) plasmid. We observed a broad level of fluorescence in *fdb* muscle, indicating expression of the fluorescent protein. Results in Fig. 3 B (representative Western blot and quantification of protein levels from three different preparations) show that the Panx1 protein level had dropped by ∼65% in muscles electroporated with the shPanx1 plasmid. This reduction in protein levels correlates with changes in ATP release in those fibers; in basal conditions, extracellular ATP levels were significantly lower in shPanx1-expressing fibers compared with control ones (Fig. 3 C, upper graph). Importantly, the high levels of ATP release observed after 20-Hz ES (Jorquera et al., 2013) were clearly reduced in shPanx1-expressing fibers (Fig. 3 C, lower graph). After 20-Hz ES of control muscle fibers, there is an increase in mRNA levels of TnIs and a decrease in mRNA levels of TnIf (Fig. 3 D), as previously reported (Jorquera et al., 2013). Nevertheless, in fibers electroporated with the shPanx1 plasmid, the electrical stimuli failed to induce these transcriptional changes. Although the basal levels of TnIs appear to be reduced in shPanx1 compared with control, they reach no statistical difference (98 ± 5.5 in controls versus 54 ± 15.7 in shPanx1 fibers, $P = 0.1$).

Down-expression of Pannexin-1 does not alter Ca^{2+} current trough $Ca_V1.1$

We previously showed that pharmacological alteration of $Ca_V1.1$ activity is associated with an altered Panx1 function (Jorquera et al., 2013). In the present work, we looked for a possible involvement of Panx1 over $Ca_V1.1$ function. We first examined the Ca^{2+} channel activity of $Ca_V1.1$ in voltage-clamped fibers down-expressing Panx1, while mCherry-expressing fibers were used

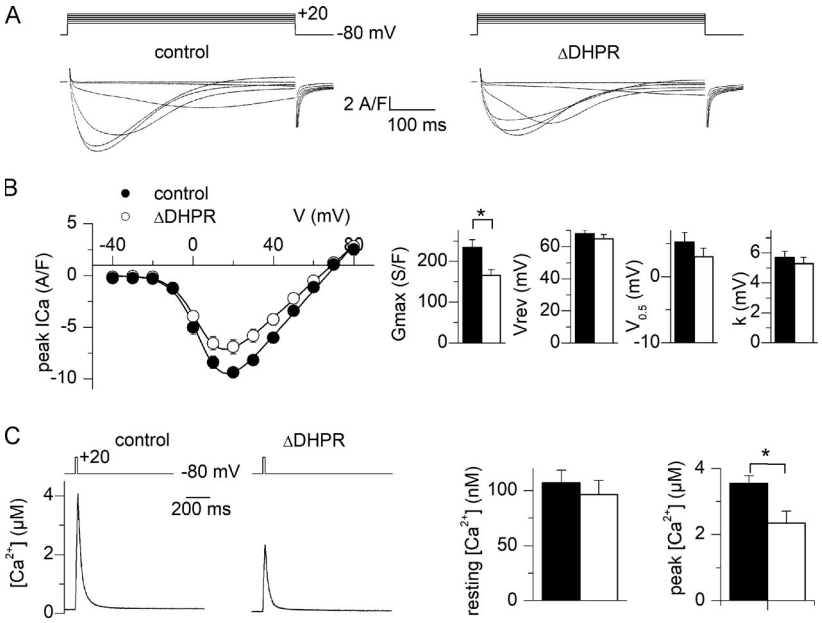

Figure 2. **Reduced voltage-activated Ca^{2+} current and intracellular Ca^{2+} release in muscle fibers down-expressing $Ca_V1.1$. (A)** Ca^{2+} current records from a control fiber (left) and a fiber down-expressing $Ca_V1.1$ (right). Currents were recorded in response to the voltage pulses shown on top. **(B)** Mean voltage dependence of the peak $Ca_V1.1$ Ca^{2+} current density in control fibers and in fibers down-expressing $Ca_V1.1$. Graphs on the right show corresponding mean values for the current–voltage parameters obtained by fitting individual series of data points with Eq. 1. **(C)** Indo-1 Ca^{2+} transient elicited by a 20-ms-long depolarizing pulse to +10 mV in a control fiber and in a fiber down-expressing $Ca_V1.1$. Graphs on the right show corresponding mean values for resting and peak $[Ca^{2+}]$ levels (results are from 14 control fibers and 14 fibers down-expressing $Ca_V1.1$ from four mice). Black circles and bars correspond to control fibers and open circles and bars to fiber down-expressing $Ca_V1.1$. Data are expressed as mean ± SEM. Nested analysis was done for data in graphs shown in B and C. *, P < 0.05.

as control, as described in Materials and methods. Mean values for the capacitance in the mCherry and in the shPanx1 groups of fibers in these experiments were 1.02 ± 0.14 (22 fibers form five different animals) and 1.22 ± 0.08 nF (21 fibers form four different animals), respectively (statistically not different). Regarding the access resistance, as explained in Materials and methods, its value is minimized by crushing the tip of the voltage-clamp micropipette once it is inserted in the silicone-embedded portion of muscle fiber. To test for a possible difference in voltage-clamp kinetics between the two groups of fibers, we fitted the decay of the capacitive transient elicited by a 20-mV hyperpolarizing voltage step with a double-exponential function. Mean values for the fast and slow time constants in the mCherry and in the shPanx1 groups were 0.77 ± 0.14 and 0.57 ± 0.09 ms and 2.52 ± 0.22 and 3.14 ± 0.55 ms (22 fibers from five animals in the control group and 21 fibers from four different

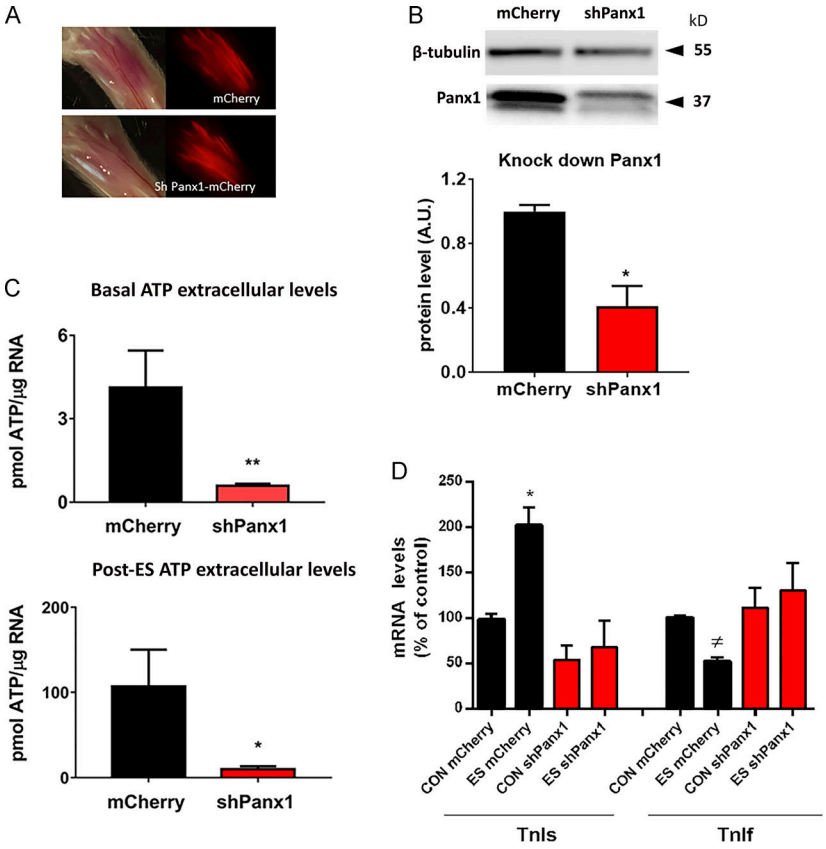

Figure 3. **Down-expression of Panx1 decreases basal and post-ES (20 Hz) levels of extracellular ATP altering ES-dependent changes in gene expression. (A)** Panel showing red fluorescent fibers after 2 wk of electroporation of *fdb* muscles with plasmid carrying mCherry (upper panel) and shPanx1-mCherry (lower panel). The corresponding transmitted light images demonstrate broad expression of both plasmids. Whole *fdb* shown is 1 cm long. **(B)** Western blots against Panx1 of *fdb* muscles shows that the muscles expressing the shRNA against Panx1 construct reduces Panx1 protein levels by ∼65% (n = 3 muscles from three distinct mice). **(C)** The reduction of Panx1 in *fdb* fibers significantly decreases basal levels of extracellular ATP (left) as well as ES-activated ATP release (right; n = 5 culture plates from five distinct mice). **(D)** 20 Hz ES-related changes in mRNA levels of TnIs and TnIf observed in mCherry fibers are suppressed in fibers knocked down for Panx1 (n = 3 distinct animals). We can observe a reduction of basal levels of TnIs mRNA in fibers knocked down for Panx1 compared with control (98 ± 5.5 in controls versus 54 ± 15.7 in shPanx1), but it reaches no statistical difference (P = 0.1). Black bars represent mCherry-expressing fibers, and red bars represent shPanx1-mCherry–expressing fibers. Significant differences within multiple groups were examined using a Kruskal–Wallis test for repeated measures, followed by a multiple comparison test. A Mann–Whitney test was used to detect significant differences between two groups. Data are expressed as mean ± SEM. */≠, P < 0.05; **, P < 0.01 versus control mCherry fibers.

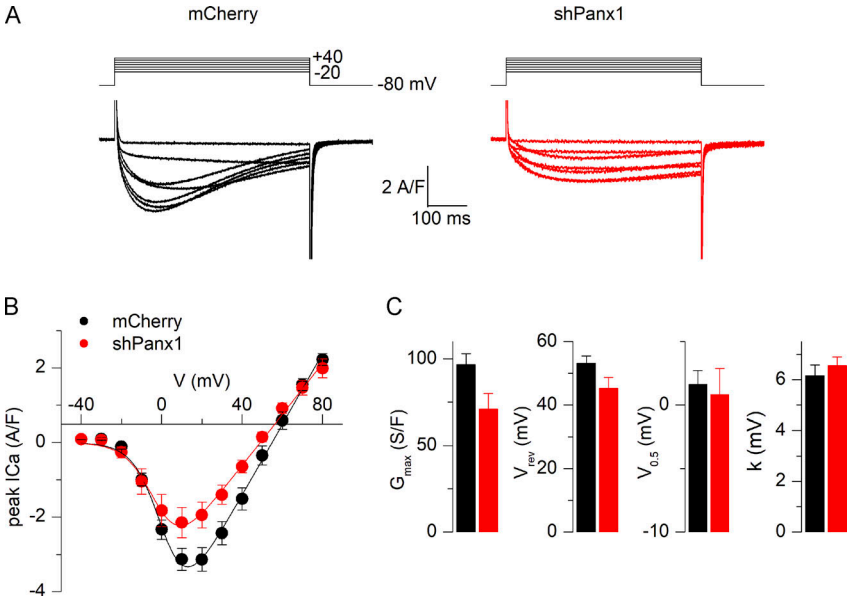

Figure 4. **Reduced expression of Pannexin-1 does not alter Ca^{2+} current through $Ca_V1.1$. (A)** Ca^{2+} current records from a control fiber (left) and from a fiber down-expressing Panx1 (right). Currents were recorded in response to the voltage pulses shown on top. **(B)** Mean voltage dependence of the peak $Ca_V1.1$ Ca^{2+} current density in control fibers and in fibers down-expressing Panx1. **(C)** Corresponding mean values for the current–voltage parameters obtained by fitting individual series of data points with Eq. 1. Mean values for the capacitance in the mCherry and in the shPanx1 groups of fibers used were 1.02 ± 0.14 and 1.22 ± 0.08 nF (n = 22 control fibers from three distinct mice and 21 fibers expressing the shRNA against Panx1 from four distinct mice). Black bars and lines represent mCherry-expressing fibers, and red bars represent shPanx1-mCherry–expressing fibers. Data are expressed as mean ± SEM. Nested analysis was done for data shown in C.

animals in the shPanx1 group), respectively (also not statistically different). Fig. 4 A shows Ca^{2+} current records from a control fiber and a fiber transfected with the shPanx1 plasmid. Records were obtained in response to 0.5-s-long depolarizing pulses from −80 mV to levels ranging between −20 and +40 mV. The peak amplitude of the current was lower in the shPanx1 condition, and the kinetics of the Ca^{2+} current also appeared slower. Fig. 4 B shows the mean peak current versus voltage relationship from measurements in 22 control fibers (from five different animals) and 21 fibers (from four different animals) expressing the shRNA against Panx1. Individual series of data points in each fiber were fitted with Eq. 1, and mean corresponding values for the parameters are reported in Fig. 4 C, showing a 27% reduction in the maximal conductance in fibers expressing the shPanx1 as compared with mCherry expressing fibers, whereas other parameters were unchanged. As each animal was electroporated in one paw with mCherry-expressing plasmid and its contralateral paw with the shPanx1 plasmid, we may consider that each fiber (even when coming from the same animal) could be considered as an independent measure rather than considered as a replicant of other fibers measured coming from the same muscle. In this case, the reduction in maximal conductance is significant (P = 0.0274). However, when compared using a nested analysis, this difference is not significant. There was no significant difference also between subcolumns of the same group. The spontaneous Ca^{2+} current decay during the large pulses also appeared slower in shPanx1 as compared with control fibers. As it was too slow to be fitted with a single exponential, we evaluated this parameter by counting the number of fibers yielding at least a half decrease of the peak current during the pulse to +20 mV. This corresponded to 81% and 33% of the control and shPanx1 fibers, respectively. Altogether, down-expression of Panx1 did not produce significant alterations in $Ca_V1.1$ Ca^{2+} current properties. Maybe more experiments would be needed to increase n values to evaluate the difference in Gmax. The size of both control and shPanx1 fibers Ca^{2+} currents is smaller than that shown in Fig. 2. This is due to the fact that 8-mo-old C57/Bl6 mice were used for experiments described in that figure as compared with 6–7-wk-old BalbC mice in Fig. 4.

Down-expression of Pannexin-1 depresses voltage-activated SR Ca^{2+}release

One critical function of the $Ca_V1.1$ protein is its role in EC coupling. We addressed the issue of whether RYR1-mediated SR Ca^{2+} release would be altered in this condition of Panx1 down-expression. Fig. 5 A shows representative fluo-4 Ca^{2+} transients elicited by a train of short depolarizing pulses of increasing amplitude in a control (mCherry) and in a shPanx1 muscle fiber. While the overall qualitative time course of change in Ca^{2+} was similar in the two fibers, the peak amplitude of the Ca^{2+} signals was severely depressed at all voltages in the shPanx1 fiber. This was a reproducible feature as shown by the voltage dependence of the mean values for peak rate of rise of fluo-4 Ca^{2+} transients in the two groups of fibers (Fig. 5 B; n = 17 [from four animals] and 21 [from three animals] control and shPanx1 fibers, respectively). Fitting a Boltzmann function to the peak rate values versus voltage in each fiber gave the mean parameters shown in the first row of the right panel in Fig. 5 B. The comparison between the two sets of data was done using nested analysis and showed a significant 57% reduction in the maximum rate of rise of fluo-4 fluorescence in the shPanx1 fibers, whereas the midpoint voltage and steepness factor were unchanged. The apparent time course of Ca^{2+} decay appeared unaffected in the shRNA-Panx1 fibers (Fig. 5 A), suggesting that SERCA-mediated Ca^{2+} uptake was properly operating in this condition. To quantitatively appreciate the cytosolic Ca^{2+} removal capabilities of the fibers, we fitted a double-exponential function to the decay of the Ca^{2+} transient after the end of the last depolarizing pulse of the protocol. The result from the fit is shown in blue superimposed to the traces in Fig. 5 A. Mean values for the time constants did not differ between control and shRNA-Panx1 fibers, but the final level was moderately but significantly

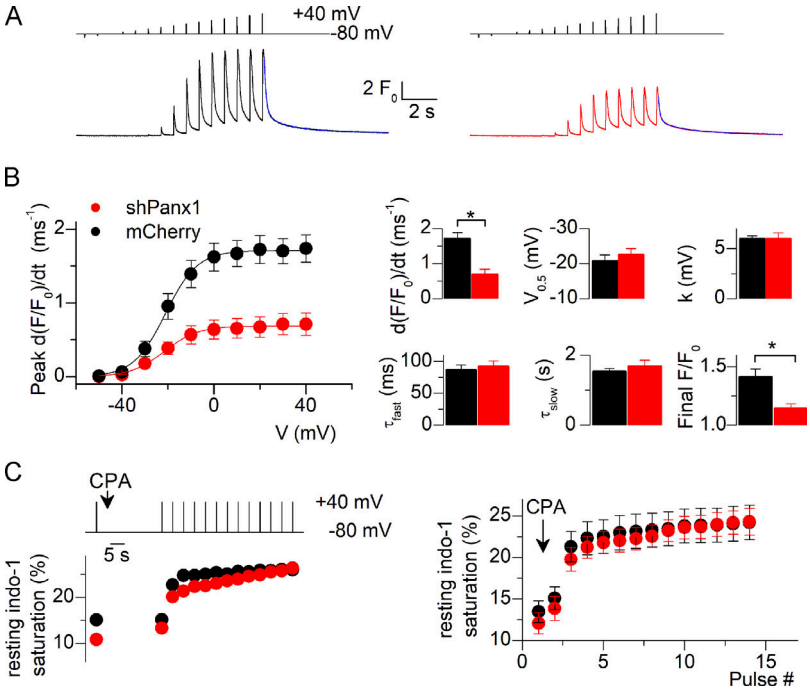

Figure 5. **Reduced expression of Pannexin-1 drastically alters voltage-activated SR Ca^{2+} release. (A)** Fluo-4 F/F_0 Ca^{2+} transients recorded from a control fiber (left) and a fiber down-expressing Panx1 (right). Transients were recorded in response to the voltage protocol shown on top. The superimposed blue line at the end of the record corresponds to the result from fitting a double-exponential plus constant function to the decay of the signal. **(B)** Voltage dependence of the mean peak rate of rising of fluo-4 fluorescence in control fibers and fibers down-expressing Panx1. Graphs in the upper row on the right show corresponding values for the Boltzmann parameters obtained from fitting individual series of data points with Eq. 2. Graphs in the bottom row on the right show mean values obtained from fitting the double-exponential plus constant function to the final decay of the fluo-4 transient. **(C)** Estimation of the SR Ca^{2+} content. Indo-1 resting saturation level was measured in control fibers and fibers down-expressing Panx1 challenged by repeated depolarizing pulses in the presence of CPA. An example of the corresponding time course of change in indo-1 saturation in a fiber from each group is shown on the left. Mean values are shown on the right (n = 12 fibers for both control and shPanx1 muscles from three distinct mice). Black bars and lines represent mCherry-expressing fibers and red bars and lines represent shPanx1-mCherry–expressing fibers. Data are expressed as mean ± SEM. *, $P < 0.05$. Nested analysis was performed in data from graphs shown in B.

depressed in the shPanx1 fibers (1.14 ± 0.04, as compared with 1.41 ± 0.07 in mCherry-expressing fibers, n = 17 (from four animals) and n = 21 (from three animals) control and shPanx1 fibers, respectively).

As the reduced peak amplitude of voltage-activated Ca^{2+} transients in shPanx1 muscle fibers may result from altered RYR1 activity or the depressed driving force for the Ca^{2+} exit because of reduced SR content, we tested whether the SR Ca^{2+} content differed between control and shPanx1 fibers. We used a protocol measuring the saturation level of the Ca^{2+}-sensitive dye indo-1 in fibers loaded with a high concentration of EGTA and challenged with repeated depolarizing pulses in the presence of CPA to release the SR Ca^{2+} contents into the cytosol (see Materials and methods). The left panel in Fig. 5 C shows the time course of resting indo-1 saturation level in a control and in a shPanx1 muscle fiber during that protocol. The right panel shows corresponding mean values obtained from 12 control fibers and 12 shPanx1 fibers muscle (n = 3 animals), respectively. There was no significant difference between the two datasets. The SR Ca^{2+} content was estimated in each fiber from the difference between the initial resting indo-1 saturation level before CPA application and the level reached at the end of the protocol, assuming 10 mM free EGTA was present in the intracellular medium and that EGTA and indo-1 have the same affinity for Ca^{2+}. This gave mean SR Ca^{2+} content values of 1.03 ± 0.13 and 1.24 ± 0.13 mM in control and shPanx1 fibers, respectively.

Intramembrane charge movement is not altered in fibers down-expressing Pannexin-1

We tested whether the changes in $Ca_V1.1$ function induced by reduced Panx1 expression were paralleled by changes in $Ca_V1.1$ voltage-sensor properties. For this, the intramembrane charge movement was compared between shPanx1 fibers and control fibers. Fig. 6 A shows representative traces of charge currents from a fiber of each group, while Fig. 6 B shows the mean voltage dependence of the charge density from 11 (from three animals) and 16 control and shPanx1 fibers (from three animals), respectively. Fitting individual series of data points in each fiber with Eq. 2 gave mean values presented in Fig. 6 C for the Boltzmann parameters. There was no difference in any parameter between control and shRNA-Panx1 fibers, demonstrating that down-expression of Panx1 did not affect the $Ca_V1.1$ intramembrane charge movement and that the decreased Ca^{2+} channel conductance reported in Fig. 4 was not the consequence of reduced $Ca_V1.1$ expression levels.

Discussion

$Ca_V1.1$ plays an essential role in skeletal muscle, and its regulation by interaction with partner proteins or protein complexes has shed light onto the very exquisite manner in which it performs and regulates its functions. In the present work, we provide evidence for bidirectional functional interaction between $Ca_V1.1$ and Panx1. Control of Panx1 activity by $Ca_V1.1$ is involved in decoding the frequency of electrical activity and transducing it into transcriptional events crucial for muscle plasticity. In return, Panx1 now appears as a compulsory partner for proper function of $Ca_V1.1$ in EC coupling.

Role of Panx1 over $Ca_V1.1$: Lessons from other $Ca_V1.1$-interacting proteins

We demonstrate here that reduced levels of Panx1 protein may alter some features of $Ca_V1.1$ function depressing activation of voltage-dependent SR Ca^{2+} release. Altered $Ca_V1.1$ activity was

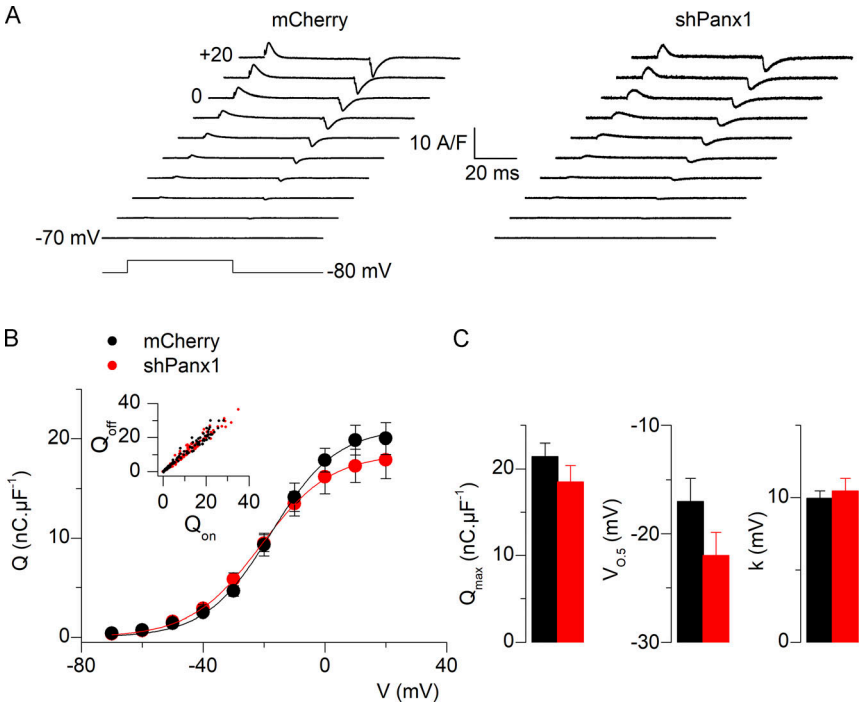

Figure 6. **Expression of shRNA against Pannexin-1 does not alter intramembrane charge movements in fibers down-expressing Pannexin-1. (A)** Illustrative traces of intramembrane charge current, Q, normalized to the fiber's capacitance (in nanocoulombs, nC, per microFarad, µF) in a control fiber (left) and a fiber down-expressing Panx1 (right). **(B)** The voltage dependence of the mean amount of charge in control fibers and fibers down-expressing Panx1. The inset shows good equality between on and off charges. **(C)** Mean values for the parameters obtained from fitting a Boltzmann function to the individual series of data points (n = 12 fibers for both control and shPanx1 muscles from four distinct mice). Black bars and lines represent mCherry-expressing fibers and red bars and lines represent shPanx1-mCherry–expressing fibers. Data are expressed as mean ± SEM.

not due to a reduced amount of the $Ca_V1.1$ protein in the t-tubule membrane (as shown in Fig. 6), as is the case, for instance, under conditions of down-expression of other proteins interacting with $Ca_V1.1$ and regulating its function (e.g., JP45 and junctophilin; Golini et al., 2011; Yasuda et al., 2013). Thus, changes in $Ca_V1.1$ activity in Ca^{2+} release must result from disruption of Panx1–$Ca_V1.1$ functional interaction and of proper organization and/or function of the $Ca_V1.1$–RYR1 interaction (EC coupling machinery), respectively. It is interesting to note here that there is no simple correlation between changes in $Ca_V1.1$ membrane content, changes in Ca^{2+} current, and voltage-dependent SR Ca^{2+} release. For instance, in junctophilin1-deficient muscle cells, there is a reduction of ∼60% of peak amplitude of Ca^{2+} transients, without changes in Ca^{2+} currents or $Ca_V1.1$ membrane content (Nakada et al., 2018). Also, in muscle fibers from JP45/CASQ1 double KO mice, there is no significant change in $Ca_V1.1$ membrane content, but there is a robust increase of 45% in the Ca^{2+} conductance (Gmax) compared with fibers from WT mice (Mosca et al., 2013). As proposed for other proteins, Panx1 could play a role in proper $Ca_V1.1$ tetrad formation. This is indeed a possibility as the functional phenotype combining reduction in $Ca_V1.1$ Ca^{2+} current and in SR Ca^{2+} release, together with preserved intramembrane charge movement, is reminiscent of what occurs either in the absence of RYR1 (Nakai et al., 1996) or in the presence of a truncated form of the β_{1a} subunit of the DHPR (Eltit et al., 2014), both conditions being associated with disorganization of the standard arrangement of $Ca_V1.1$s in tetrad arrays (Eltit et al., 2014; Protasi et al., 1998). Accordingly, it may be that loss of Panx1 also contributes to disentangle the arrays to affect both orthograde and retrograde $Ca_V1.1$–RYR1 signaling.

From a more general point of view, we cannot exclude that the reduction of voltage-activated SR Ca^{2+} release associated with Panx1 knockdown results from altered expression of one or several key proteins of the EC coupling machinery. Except from results from the charge movement experiments that limit the likelihood that the $Ca_V1.1$ expression level is affected, we cannot completely exclude that it is not the case for RYR1, Stac3, the β1 subunit of the DHPR, or another critical component of the machinery.

Role of $Ca_V1.1$ over Panx1

We previously showed that $Ca_V1.1$ activates ATP release upon 20-Hz ES in adult muscle fibers, leading to the activation of a signaling cascade related to muscle plasticity (Jorquera et al., 2013). Our present results demonstrate that, in addition to the control of $Ca_V1.1$ over Panx1, there is also a control of $Ca_V1.1$ by Panx1, through which Panx1 deficiency leads to dysfunction of $Ca_V1.1$ effect in EC coupling.

The functional interaction between $Ca_V1.1$ and Panx1 is important not only for activation of Panx1 following electrical activity. Indeed, in resting conditions, the interaction also controls basal levels of ATP release. We previously reported that dysgenic myotubes (lacking $Ca_V1.1$) have increased levels of extracellular ATP release in basal conditions (Jorquera et al., 2013). We now show that in these cells the high level of ATP release is due to Panx1 activity (see Fig. 1). Importantly, we also show that knockdown of $Ca_V1.1$ by a U7 exon–skipping strategy in differentiated fibers also results in an increased resting level of ATP release and altered expression of TnI isoforms. This suggests that, in these conditions, increased resting ATP release is sufficient to activate signaling pathways related to muscle plasticity in control muscle fibers.

The control of Panx1 by $Ca_V1.1$ in resting conditions is also important in some muscular disorders. In the mdx mouse model of Duchenne muscular dystrophy, there is a loss of negative control of ATP release in resting conditions (Valladares et al., 2013). The fact that the $Ca_V1.1$ blocker nifedipine improves the muscular function of mdx mice (Altamirano et al., 2013) highlights the importance of the above-mentioned interaction in this pathological muscle condition. Also, since there is evidence that

Ca^{2+} release is depressed in mdx muscle fibers (Hollingworth et al., 2008; Woods et al., 2004), it could be speculated that this occurs, at least in part, because of the reduced interaction between $Ca_V1.1$ and Panx1. We expected that lack of $Ca_V1.1$ would have no effect or even decrease Panx1 activity, but experimentally, the reduction in $Ca_V1.1$ expression resulted in increased Panx1 activity, suggesting an inhibitory effect of $Ca_V1.1$ on Panx1-mediated permeation at rest.

Reduction in Panx1 decreased depolarization-induced Ca^{2+} release in the absence of SR Ca^{2+} depletion, suggesting that the lessening of Panx1 content could alter $Ca_V1.1$'s relationship with RYR1 in skeletal muscle fibers. Panx1 may be a good candidate to study in other models of dystrophies because the loss of Panx1 causes a deficient depolarization-induced Ca^{2+} release that could contribute to muscle weakness present in several muscle pathologies (Jorquera et al., 2021). Altogether, $Ca_V1.1$–Panx1 interactions are essential for activation of gene transcription related to muscle plasticity, but they also may play an important role in certain muscle disorders, pointing to $Ca_V1.1$ as a potential target for the development of therapies.

Direct molecular interaction?

Even if the existence of a direct molecular interaction between $Ca_V1.1$ and Panx1 may be the simplest explanation for our results, we must be cautious in recognizing this interaction between $Ca_V1.1$ and Panx1 has not been fully demonstrated or molecularly mapped, although is suggested by the experimental evidence (coimmunoprecipitation, colocalization using proximity ligation assay, comigration in the same protein complex; Arias-Calderón et al., 2016; Jorquera et al., 2013). The present results suggest that the protein complex involved in EC coupling ($Ca_V1.1$ and RYR1) also includes Panx1, as Panx1 and $Ca_V1.1$ have been identified, together with P2Y, to be part of the above-mentioned macromolecular complex (Arias-Calderón et al., 2016). Arias-Calderón et al. proposed that there are two different complexes along the t-tubule membrane, one near the surface membrane that includes (besides $Ca_V1.1$, Panx1, and P2Y2) caveolin3 and possibly dystrophin and one that spans all the length of the t-tubule that includes P2Y2 and $Ca_V1.1$ and that, according to the present results and its known location, should also include RYR1. The location of Panx1 was not clearly determined in the Arias-Calderón et al. study, but upon a close look to the immunofluorescence images they show, Panx1 should also be considered in a complex that spans all the t-tubule length.

The apparent inhomogeneity of Panx1 along the t-tubule may be explained by the incapability of biochemical and localization assays to discriminate between immature and/or nonfunctional pool of proteins or by a lack of sensitivity of the antibodies to detect Panx1 in the center of the fiber. The effect we see on Ca^{2+} release could also be related to a nonlinear release along the cross section of the fiber or an additional adaptive response mediated by signaling events provoked by the decrease in Panx1 as a secondary effect on the EC coupling machinery.

Panx1-related disorders beyond the muscle

It is known that Panx1 channels are important in many organs. A case of a human autosomal recessive Panx1 missense gene variant exhibited intellectual disability and severe hearing loss, along with deficits in other organ systems including the skeleton (Shao et al., 2016). This gene variant consisted of an arginine to histidine substitution at position 217 (p.Arg217His) which was shown to reduce channel currents, dye flux, and ATP release while preserving surface expression. The severity of the impairments/disabilities observed are in apparent contradiction with the relatively modest phenotype in Panx1 KO mice. This modest phenotype has been speculated to be the result of compensation for the global loss of Panx1 from conception to adulthood. Indeed, evidence of compensation (by Panx3) in global Panx1 KO mice has been demonstrated (Lohman and Isakson, 2014; Whyte-Fagundes et al., 2018).

An interaction between Panx1 and other Ca_V channels has been suggested. $Ca_V1.2$ is present and functional in other tissues like lungs, where it was found that clevidipine, used to lower blood pressure, has an increased effect over $Ca_V1.2$ when Panx1 is present (Dahl et al., 2016). This may have an important clinical consequence because it would support the use of this dihydropyridine to reduce breathing problems and possibly also in the treatment of acute heart failure (Dahl et al., 2016). Thus, the functional interaction between Ca_V1 and Panx1 appears to be crucial not only for skeletal muscle but also for other tissues. Considering the widespread expression of Panx1 together with the presence of different members of the Ca_V family in heart, brain, and smooth muscle, we speculate that functional interaction between the two may be relevant in several physiological and pathological conditions.

Acknowledgments

Eduardo Ríos served as editor.

We thank Jorge Hidalgo for his help in establishing and maintaining the electrophysiological setup in Chile and helpful discussion and comments throughout the project. We thank Mónica Silva for help with the preparation of isolated muscle fibers. Measurements of intramembrane charge movement (Fig. 6) and SR Ca^{2+} content (Fig. 5 C) and Ca^{2+} current and Ca^{2+} transients in muscle fibers down-expressing $Ca_V1.1$ (Fig. 2) were performed at Institut NeuroMyoGène, University Claude Bernard, Lyon 1. Measurements of DHPR protein level, ATP levels, and gene expression in fibers down-expressing $Ca_V1.1$ (Fig. 1) were performed at Institut de Myologie, Université Paris 6. All other experiments were performed at the Muscle Physiology Laboratory, Instituto de Ciencias Biomédicas, University of Chile.

This work was supported by the Chilean-French cooperation program ECOS-CONICYT (Comisión Nacional de Investigación Científica y Tecnológica [Chile], Comité d'Evaluation-Orientation de la Coopération Scientifique [ECOS]; grant C13B01); Fondo Nacional de Desarrollo Científico y Tecnológico (grant 1151293 and postdoctoral fellowship 3170194 to G. Jorquera); Comisión Nacional de Investigación Científica y Tecnológica (CONICYT, Chile) (fellowship 21130284 to J. Troc-Gajardo); and Centre National de la Recherche Scientifique, Institut National de la Santé et de la Recherche Médicale, University Claude Bernard Lyon 1, and Association Française contre les Myopathies (AFM-Téléthon) grants to the Institut NeuroMyoGène.

The authors declare no competing financial interests.

Author contributions: F. Jaque-Fernández, G. Jorquera, M. Casas, and V. Jacquemond performed experiments, analyzed

results, and assembled figures. J. Troc-Gajardo, S. Buvinic, and B. Allard performed experiments and analyzed results. C. Gentil performed experiments. F. Pietri-Rouxel contributed to design the experimental strategy, planned experiments, and analyzed results. E. Jaimovich planned experiments, discussed results, and revised the manuscript. M. Casas and V. Jacquemond designed the project, planned the experiments, and wrote the manuscript. All authors approved the final version of the manuscript and agree to be accountable for all aspects of the work in ensuring that questions related to the accuracy or integrity of any part of the work are appropriately investigated and resolved. All persons designated as authors qualify for authorship, and all those who qualify for authorship are listed.

Submitted: 21 April 2020
Revised: 24 May 2021
Accepted: 15 September 2021

References

Al-Qusairi, L., N. Weiss, A. Toussaint, C. Berbey, N. Messaddeq, C. Kretz, D. Sanoudou, A.H. Beggs, B. Allard, J.-L. Mandel, et al. 2009. T-tubule disorganization and defective excitation-contraction coupling in muscle fibers lacking myotubularin lipid phosphatase. *Proc. Natl. Acad. Sci. USA.* 106:18763–18768. https://doi.org/10.1073/pnas.0900705106

Altamirano, F., D. Valladares, C. Henríquez-Olguín, M. Casas, J.R. López, P.D. Allen, and E. Jaimovich. 2013. Nifedipine treatment reduces resting calcium concentration, oxidative and apoptotic gene expression, and improves muscle function in dystrophic mdx mice. *PLoS One.* 8:e81222. https://doi.org/10.1371/journal.pone.0081222

Anderson, A.A., X. Altafaj, Z. Zheng, Z.M. Wang, O. Delbono, M. Ronjat, S. Treves, and F. Zorzato. 2006. The junctional SR protein JP-45 affects the functional expression of the voltage-dependent Ca2+ channel Cav1.1. *J. Cell Sci.* 119:2145–2155. https://doi.org/10.1242/jcs.02935

Andronache, Z., S.L. Hamilton, R.T. Dirksen, and W. Melzer. 2009. A retrograde signal from RyR1 alters DHP receptor inactivation and limits window Ca^{2+} release in muscle fibers of Y522S RyR1 knock-in mice. *Proc. Natl. Acad. Sci. USA.* 106:4531–4536. https://doi.org/10.1073/pnas.0812661106

Arias-Calderón, M., G. Almarza, A. Díaz-Vegas, A. Contreras-Ferrat, D. Valladares, M. Casas, H. Toledo, E. Jaimovich, and S. Buvinic. 2016. Characterization of a multiprotein complex involved in excitation-transcription coupling of skeletal muscle. *Skelet. Muscle.* 6:15. https://doi.org/10.1186/s13395-016-0087-5

Bannister, R.A., and K.G. Beam. 2009. Ryanodine modification of RyR1 retrogradely affects L-type Ca^{2+} channel gating in skeletal muscle. *J. Muscle Res. Cell Motil.* 30:217–223. https://doi.org/10.1007/s10974-009-9190-0

Bao, L., S. Locovei, and G. Dahl. 2004. Pannexin membrane channels are mechanosensitive conduits for ATP. *FEBS Lett.* 572:65–68. https://doi.org/10.1016/j.febslet.2004.07.009

Baranova, A., D. Ivanov, N. Petrash, A. Pestova, M. Skoblov, I. Kelmanson, D. Shagin, S. Nazarenko, E. Geraymovych, O. Litvin, et al. 2004. The mammalian pannexin family is homologous to the invertebrate innexin gap junction proteins. *Genomics.* 83:706–716. https://doi.org/10.1016/j.ygeno.2003.09.025

Beam, K.G., and R.A. Bannister. 2010. Looking for answers to EC coupling's persistent questions. *J. Gen. Physiol.* 136:7–12. https://doi.org/10.1085/jgp.201010461

Buvinic, S., G. Almarza, M. Bustamante, M. Casas, J. López, M. Riquelme, J.C. Sáez, J.P. Huidobro-Toro, and E. Jaimovich. 2009. ATP released by electrical stimuli elicits calcium transients and gene expression in skeletal muscle. *J. Biol. Chem.* 284:34490–34505. https://doi.org/10.1074/jbc.M109.057315

Casas, M., R. Figueroa, G. Jorquera, M. Escobar, J. Molgó, and E. Jaimovich. 2010. IP_3-dependent, post-tetanic calcium transients induced by electrostimulation of adult skeletal muscle fibers. *J. Gen. Physiol.* 136:455–467. https://doi.org/10.1085/jgp.200910397

Casas, M., S. Buvinic, and E. Jaimovich. 2014. ATP signaling in skeletal muscle: from fiber plasticity to regulation of metabolism. *Exerc. Sport Sci. Rev.* 42:110–116. https://doi.org/10.1249/JES.0000000000000017

Chekeni, F.B., M.R. Elliott, J.K. Sandilos, S.F. Walk, J.M. Kinchen, E.R. Lazarowski, A.J. Armstrong, S. Penuela, D.W. Laird, G.S. Salvesen, et al. 2010. Pannexin 1 channels mediate 'find-me' signal release and membrane permeability during apoptosis. *Nature.* 467:863–867. https://doi.org/10.1038/nature09413

Collet, C., L. Csernoch, and V. Jacquemond. 2003. Intramembrane charge movement and L-type calcium current in skeletal muscle fibers isolated from control and mdx mice. *Biophys. J.* 84:251–265. https://doi.org/10.1016/S0006-3495(03)74846-2

Corriden, R., and P.A. Insel. 2010. Basal release of ATP: an autocrine-paracrine mechanism for cell regulation. *Sci. Signal.* 3:re1. https://doi.org/10.1126/scisignal.3104re1

Couchoux, H., B. Allard, C. Legrand, V. Jacquemond, and C. Berthier. 2007. Loss of caveolin-3 induced by the dystrophy-associated P104L mutation impairs L-type calcium channel function in mouse skeletal muscle cells. *J. Physiol.* 580:745–754. https://doi.org/10.1113/jphysiol.2006.124198

Dahl, G.P., G.E. Conner, F. Qiu, J. Wang, E. Spindler, J.A. Campagna, and H.P. Larsson. 2016. High affinity complexes of pannexin channels and L-type calcium channel splice-variants in human lung: Possible role in clevidipine-induced dyspnea relief in acute heart failure. *EBioMedicine.* 10:291–297. https://doi.org/10.1016/j.ebiom.2016.06.027

Dayal, A., K. Schrötter, Y. Pan, K. Föhr, W. Melzer, and M. Grabner. 2017. The Ca^{2+} influx through the mammalian skeletal muscle dihydropyridine receptor is irrelevant for muscle performance. *Nat. Commun.* 8:475. https://doi.org/10.1038/s41467-017-00629-x

D'hondt, C., R. Ponsaerts, H. De Smedt, M. Vinken, E. De Vuyst, M. De Bock, N. Wang, V. Rogiers, L. Leybaert, B. Himpens, and G. Bultynck. 2011. Pannexin channels in ATP release and beyond: an unexpected rendezvous at the endoplasmic reticulum. *Cell. Signal.* 23:305–316. https://doi.org/10.1016/j.cellsig.2010.07.018

Eisner, D.A. 2021. Pseudoreplication in physiology: More means less. *J Gen. Physiol.* 153:e202012826. https://doi.org/10.1085/jgp.202012826

Eltit, J.M., C. Franzini-Armstrong, and C.F. Perez. 2014. Amino acid residues 489-503 of dihydropyridine receptor (DHPR) β1a subunit are critical for structural communication between the skeletal muscle DHPR complex and type 1 ryanodine receptor. *J. Biol. Chem.* 289:36116–36124. https://doi.org/10.1074/jbc.M114.615526

Estève, E., J.M. Eltit, R.A. Bannister, K. Liu, I.N. Pessah, K.G. Beam, P.D. Allen, and J.R. López. 2010. A malignant hyperthermia-inducing mutation in RYR1 (R163C): alterations in Ca^{2+} entry, release, and retrograde signaling to the DHPR. *J. Gen. Physiol.* 135:619–628. https://doi.org/10.1085/jgp.200910328

Gallot, Y.S., J.D. McMillan, G. Xiong, K.R. Bohnert, A.R. Straughn, B.G. Hill, and A. Kumar. 2017. Distinct roles of TRAF6 and TAK1 in the regulation of adipocyte survival, thermogenesis program, and high-fat diet-induced obesity. *Oncotarget.* 8:112565–112583. https://doi.org/10.18632/oncotarget.22575

Georgiou, D.K., A. Dagnino-Acosta, C.S. Lee, D.M. Griffin, H. Wang, W.R. Lagor, R.G. Pautler, R.T. Dirksen, and S.L. Hamilton. 2015. Ca^{2+}binding/permeation via calcium channel, $Ca_V1.1$, regulates the intracellular distribution of the fatty acid transport protein, CD36, and fatty acid metabolism. *J. Biol. Chem.* 290:23751–23765. https://doi.org/10.1074/jbc.M115.643544

Golini, L., C. Chouabe, C. Berthier, V. Cusimano, M. Fornaro, R. Bonvallet, L. Formoso, E. Giacomello, V. Jacquemond, and V. Sorrentino. 2011. Junctophilin 1 and 2 proteins interact with the L-type Ca^{2+} channel dihydropyridine receptors (DHPRs) in skeletal muscle. *J. Biol. Chem.* 286:43717–43725. https://doi.org/10.1074/jbc.M111.292755

Hollingworth, S., U. Zeiger, and S.M. Baylor. 2008. Comparison of the myoplasmic calcium transient elicited by an action potential in intact fibres of mdx and normal mice. *J. Physiol.* 586:5063–5075. https://doi.org/10.1113/jphysiol.2008.160507

Horowicz, P., and M.F. Schneider. 1981. Membrane charge moved at contraction thresholds in skeletal muscle fibres. *J. Physiol.* 314:595–633. https://doi.org/10.1113/jphysiol.1981.sp013726

Hu, H., Z. Wang, R. Wei, G. Fan, Q. Wang, K. Zhang, and C.C. Yin. 2015. The molecular architecture of dihydropyrindine receptor/L-type Ca^{2+} channel complex. *Sci. Rep.* 5:8370. https://doi.org/10.1038/srep08370

Jacquemond, V. 1997. Indo-1 fluorescence signals elicited by membrane depolarization in enzymatically isolated mouse skeletal muscle fibers. *Biophys. J.* 73:920–928. https://doi.org/10.1016/S0006-3495(97)78124-4

Jorquera, G., R. Meneses-Valdés, G. Rosales-Soto, D. Valladares-Ide, C. Campos, M. Silva-Monasterio, P. Llanos, G. Cruz, E. Jaimovich, and M. Casas. 2021. High extracellular ATP levels released through pannexin-1 channels mediate inflammation and insulin resistance in skeletal muscle fibres of diet-induced obese mice. *Diabetologia.* 64:1389–1401. https://doi.org/10.1007/s00125-021-05418-2

Jorquera, G., F. Altamirano, A. Contreras-Ferrat, G. Almarza, S. Buvinic, V. Jacquemond, E. Jaimovich, and M. Casas. 2013. Cav1.1 controls frequency-dependent

events regulating adult skeletal muscle plasticity. *J. Cell Sci.* 126: 1189–1198. https://doi.org/10.1242/jcs.116855

Lee, C.S., A. Dagnino-Acosta, V. Yarotskyy, A. Hanna, A. Lyfenko, M. Knoblauch, D.K. Georgiou, R.A. Poché, M.W. Swank, C. Long, et al. 2015. Ca^{2+} permeation and/or binding to CaV1.1 fine-tunes skeletal muscle Ca^{2+} signaling to sustain muscle function. *Skelet. Muscle.* 5:4. https://doi.org/10.1186/s13395-014-0027-1

Legrand, C., E. Giacomello, C. Berthier, B. Allard, V. Sorrentino, and V. Jacquemond. 2008. Spontaneous and voltage-activated Ca^{2+} release in adult mouse skeletal muscle fibres expressing the type 3 ryanodine receptor. *J. Physiol.* 586:441–457. https://doi.org/10.1113/jphysiol.2007.145862

Locovei, S., J. Wang, and G. Dahl. 2006. Activation of pannexin 1 channels by ATP through P2Y receptors and by cytoplasmic calcium. *FEBS Lett.* 580: 239–244. https://doi.org/10.1016/j.febslet.2005.12.004

Lohman, A.W., and B.E. Isakson. 2014. Differentiating connexin hemichannels and pannexin channels in cellular ATP release. *FEBS Lett.* 588: 1379–1388. https://doi.org/10.1016/j.febslet.2014.02.004

Melhorn, M.I., A.S. Brodsky, J. Estanislau, J.A. Khoory, B. Illigens, I. Hamachi, Y. Kurishita, A.D. Fraser, A. Nicholson-Weller, E. Dolmatova, et al. 2013. CR1-mediated ATP release by human red blood cells promotes CR1 clustering and modulates the immune transfer process. *J. Biol. Chem.* 288:31139–31153. https://doi.org/10.1074/jbc.M113.486035

Mormeneo, E., C. Jimenez-Mallebrera, X. Palomer, V. De Nigris, M. Vázquez-Carrera, A. Orozco, A. Nascimento, J. Colomer, C. Lerín, and A.M. Gómez-Foix. 2012. PGC-1α induces mitochondrial and myokine transcriptional programs and lipid droplet and glycogen accumulation in cultured human skeletal muscle cells. *PLoS One.* 7:e29985. https://doi.org/10.1371/journal.pone.0029985

Mosca, B., O. Delbono, M. Laura Messi, L. Bergamelli, Z.M. Wang, M. Vukcevic, R. Lopez, S. Treves, M. Nishi, H. Takeshima, et al. 2013. Enhanced dihydropyridine receptor calcium channel activity restores muscle strength in JP45/CASQ1 double knockout mice. *Nat. Commun.* 4:1541. https://doi.org/10.1038/ncomms2496

Nakada, T., T. Kashihara, M. Komatsu, K. Kojima, T. Takeshita, and M. Yamada. 2018. Physical interaction of junctophilin and the $Ca_V1.1$ C terminus is crucial for skeletal muscle contraction. *Proc. Natl. Acad. Sci. USA.* 115:4507–4512. https://doi.org/10.1073/pnas.1716649115

Nakai, J., R.T. Dirksen, H.T. Nguyen, I.N. Pessah, K.G. Beam, and P.D. Allen. 1996. Enhanced dihydropyridine receptor channel activity in the presence of ryanodine receptor. *Nature.* 380:72–75. https://doi.org/10.1038/380072a0

Nishida, M., Y. Sato, A. Uemura, Y. Narita, H. Tozaki-Saitoh, M. Nakaya, T. Ide, K. Suzuki, K. Inoue, T. Nagao, and H. Kurose. 2008. P2Y6 receptor-Galpha12/13 signalling in cardiomyocytes triggers pressure overload-induced cardiac fibrosis. *EMBO J.* 27:3104–3115. https://doi.org/10.1038/emboj.2008.237

Paolini, C., J.D. Fessenden, I.N. Pessah, and C. Franzini-Armstrong. 2004. Evidence for conformational coupling between two calcium channels. *Proc. Natl. Acad. Sci. USA.* 101:12748–12752. https://doi.org/10.1073/pnas.0404836101

Pelegrin, P., and A. Surprenant. 2006. Pannexin-1 mediates large pore formation and interleukin-1beta release by the ATP-gated P2X7 receptor. *EMBO J.* 25:5071–5082. https://doi.org/10.1038/sj.emboj.7601378

Perni, S., M. Lavorato, and K.G. Beam. 2017. De novo reconstitution reveals the proteins required for skeletal muscle voltage-induced Ca^{2+} release. *Proc. Natl. Acad. Sci. USA.* 114:13822–13827. https://doi.org/10.1073/pnas.1716461115

Piétri-Rouxel, F., C. Gentil, S. Vassilopoulos, D. Baas, E. Mouisel, A. Ferry, A. Vignaud, C. Hourdé, I. Marty, L. Schaeffer, et al. 2010. DHPR alpha1S subunit controls skeletal muscle mass and morphogenesis. *EMBO J.* 29: 643–654. https://doi.org/10.1038/emboj.2009.366

Polster, A., B.R. Nelson, E.N. Olson, and K.G. Beam. 2016. Stac3 has a direct role in skeletal muscle-type excitation-contraction coupling that is disrupted by a myopathy-causing mutation. *Proc. Natl. Acad. Sci. USA.* 113:10986–10991. https://doi.org/10.1073/pnas.1612441113

Pouvreau, S., B. Allard, C. Berthier, and V. Jacquemond. 2004. Control of intracellular calcium in the presence of nitric oxide donors in isolated skeletal muscle fibres from mouse. *J. Physiol.* 560:779–794. https://doi.org/10.1113/jphysiol.2004.072397

Protasi, F., C. Franzini-Armstrong, and P.D. Allen. 1998. Role of ryanodine receptors in the assembly of calcium release units in skeletal muscle. *J. Cell Biol.* 140:831–842. https://doi.org/10.1083/jcb.140.4.831

Rebbeck, R.T., Y. Karunasekara, P.G. Board, N.A. Beard, M.G. Casarotto, and A.F. Dulhunty. 2014. Skeletal muscle excitation-contraction coupling: who are the dancing partners? *Int. J. Biochem. Cell Biol.* 48:28–38. https://doi.org/10.1016/j.biocel.2013.12.001

Rios, E., and G. Brum. 1987. Involvement of dihydropyridine receptors in excitation-contraction coupling in skeletal muscle. *Nature.* 325:717–720. https://doi.org/10.1038/325717a0

Ríos, E., and G. Pizarro. 1991. Voltage sensor of excitation-contraction coupling in skeletal muscle. *Physiol. Rev.* 71:849–908. https://doi.org/10.1152/physrev.1991.71.3.849

Robin, G., and B. Allard. 2015. Voltage-gated Ca^{2+} influx through L-type channels contributes to sarcoplasmic reticulum Ca^{2+} loading in skeletal muscle. *J. Physiol.* 593:4781–4797. https://doi.org/10.1113/JP270252

Romanov, R.A., O.A. Rogachevskaja, M.F. Bystrova, P. Jiang, R.F. Margolskee, and S.S. Kolesnikov. 2007. Afferent neurotransmission mediated by hemichannels in mammalian taste cells. *EMBO J.* 26:657–667. https://doi.org/10.1038/sj.emboj.7601526

Samsó, M. 2015. 3D Structure of the Dihydropyridine Receptor of Skeletal Muscle. *Eur. J. Transl. Myol.* 25:4840. https://doi.org/10.4081/ejtm.2015.4840

Schneider, M.F. 1994. Control of calcium release in functioning skeletal muscle fibers. *Annu. Rev. Physiol.* 56:463–484. https://doi.org/10.1146/annurev.ph.56.030194.002335

Shao, Q., K. Lindstrom, R. Shi, J. Kelly, A. Schroeder, J. Juusola, K.L. Levine, J.L. Esseltine, S. Penuela, M.F. Jackson, and D.W. Laird. 2016. A germline variant in the PANX1 gene has reduced channel function and is associated with multisystem dysfunction. *J. Biol. Chem.* 291:12432–12443. https://doi.org/10.1074/jbc.M116.717934

Silverman, W.R., J.P. de Rivero Vaccari, S. Locovei, F. Qiu, S.K. Carlsson, E. Scemes, R.W. Keane, and G. Dahl. 2009. The pannexin 1 channel activates the inflammasome in neurons and astrocytes. *J. Biol. Chem.* 284: 18143–18151. https://doi.org/10.1074/jbc.M109.004804

Sridharan, M., S.P. Adderley, E.A. Bowles, T.M. Egan, A.H. Stephenson, M.L. Ellsworth, and R.S. Sprague. 2010. Pannexin 1 is the conduit for low oxygen tension-induced ATP release from human erythrocytes. *Am. J. Physiol. Heart Circ. Physiol.* 299:H1146–H1152. https://doi.org/10.1152/ajpheart.00301.2010

Tanabe, T., K.G. Beam, B.A. Adams, T. Niidome, and S. Numa. 1990. Regions of the skeletal muscle dihydropyridine receptor critical for excitation-contraction coupling. *Nature.* 346:567–569. https://doi.org/10.1038/346567a0

Thompson, R.J., N. Zhou, and B.A. MacVicar. 2006. Ischemia opens neuronal gap junction hemichannels. *Science.* 312:924–927. https://doi.org/10.1126/science.1126241

Thompson, R.J., M.F. Jackson, M.E. Olah, R.L. Rungta, D.J. Hines, M.A. Beazely, J.F. MacDonald, and B.A. MacVicar. 2008. Activation of pannexin-1 hemichannels augments aberrant bursting in the hippocampus. *Science.* 322:1555–1559. https://doi.org/10.1126/science.1165209

Valladares, D., G. Almarza, A. Contreras, M. Pavez, S. Buvinic, E. Jaimovich, and M. Casas. 2013. Electrical stimuli are anti-apoptotic in skeletal muscle via extracellular ATP. Alteration of this signal in Mdx mice is a likely cause of dystrophy. *PLoS One.* 8:e75340. https://doi.org/10.1371/journal.pone.0075340

Weiss, N., H. Couchoux, C. Legrand, C. Berthier, B. Allard, and V. Jacquemond. 2008. Expression of the muscular dystrophy-associated caveolin-3(P104L) mutant in adult mouse skeletal muscle specifically alters the Ca^{2+} channel function of the dihydropyridine receptor. *Pflugers Arch.* 457:361–375. https://doi.org/10.1007/s00424-008-0528-z

Weiss, N., C. Legrand, S. Pouvreau, H. Bichraoui, B. Allard, G.W. Zamponi, M. De Waard, and V. Jacquemond. 2010. In vivo expression of G-protein beta1gamma2 dimer in adult mouse skeletal muscle alters L-type calcium current and excitation-contraction coupling. *J. Physiol.* 588: 2945–2960. https://doi.org/10.1113/jphysiol.2010.191593

Whyte-Fagundes, P., S. Kurtenbach, C. Zoidl, V.I. Shestopalov, P.L. Carlen, and G. Zoidl. 2018. A potential compensatory role of Panx3 in the VNO of a Panx1 knock out mouse model. *Front. Mol. Neurosci.* 11:135. https://doi.org/10.3389/fnmol.2018.00135

Woods, C.E., D. Novo, M. DiFranco, and J.L. Vergara. 2004. The action potential-evoked sarcoplasmic reticulum calcium release is impaired in mdx mouse muscle fibres. *J. Physiol.* 557:59–75. https://doi.org/10.1113/jphysiol.2004.061291

Yasuda, T., O. Delbono, Z.M. Wang, M.L. Messi, T. Girard, A. Urwyler, S. Treves, and F. Zorzato. 2013. JP-45/JSRP1 variants affect skeletal muscle excitation-contraction coupling by decreasing the sensitivity of the dihydropyridine receptor. *Hum. Mutat.* 34:184–190. https://doi.org/10.1002/humu.22209